INSTITUTE OF PHYSICS PUBLISHING JOURNAL OF PHYSICS: CONDENSED MATTER

J. Phys.: Condens. Matter **16** (2004) 4357–4372 PII: S0953-8984(04)76485-1

# Nickel ferrite nanoparticles: elaboration in polyol medium via hydrolysis, and magnetic properties

**S Chkoundali[1], S Ammar[1], N Jouini[1,2], F Fiévet[1], P Molinié[3], M Danot[3], F Villain[4,5] and J-M Grenèche[6]**

[1] ITODYS, UMR-CNRS 7086, Université Paris 7, 2 Place Jussieu (case 7090), 75251 Paris, France
[2] LPMTM, UPR-CNRS 9001, Institut Galilée, 99 Avenue J-B Clément, 93430 Villetaneuse, France
[3] Institut Jean Rouxel des Matériaux, 2 Chemin de la Houssinière, 44072 Nantes, France
[4] LI2M, UMR-CNRS 7071, Université Paris 6, 4 Place Jussieu (case 42), 75252 Paris, France
[5] LURE, UMR-CNRS 130, Université Paris 11, BP 34, 91898 Orsay, France
[6] LPEC, UMR-CNRS 6087, Université du Maine, Avenue O Messiaen, 72085 Le Mans, France

E-mail: ammarmer@ccr.jussieu.fr

Received 18 February 2004
Published 4 June 2004
Online at stacks.iop.org/JPhysCM/16/4357
doi:10.1088/0953-8984/16/24/017

**Abstract**

Ultrafine magnetic nickel ferrite $NiFe_2O_4$ particles of high crystallinity were directly prepared by forced hydrolysis of ionic iron (III) and nickel (II) solutions in 2-hydroxyethyl ether at about 478 K under atmospheric pressure. The resulting nickel ferrite particles exhibit very interesting magnetic properties: they are superparamagnetic at room temperature and have a saturation magnetization close to that of the bulk at low temperature. An in-field Mössbauer study shows clearly that this surprising behaviour is mainly due to: (i) a departure of the cation distribution from the classical distribution encountered in the bulk material and (ii) the absence of spin canting for both tetrahedral and octahedral cations.

(Some figures in this article are in colour only in the electronic version)

## 1. Introduction

The increasing demand for oxide nanomaterials in the wide field of nanotechnology has motivated considerable research on their preparation. In this context, a great number of novel synthetic routes have been described: ball milling [1], co-precipitation [2], sonochemical [3], microwave plasma [4], co-precipitation in reverse micelle [5], sol–gel [6, 7], and near-critical and supercritical hydrothermal [8] methods. Compared to the ceramic routes, these new methods appear to be promising. Indeed, they make it possible to decrease the particle size down to the nanometre range leading to a drastic change in physical properties. Among these

  

properties, the magnetic ones are the subject of numerous studies due to the potential application of magnetic nanoparticles to high density magnetic storage media, drug delivery, etc. However, several physical phenomena exhibited by magnetic nanomaterials severely limit their use. Nanoparticles show unstable spontaneous magnetization at room temperature, because of their superparamagnetic character, and present reduced magnetization at low temperature due to surface spin disorder.

Over the past decade it has been shown that a great variety of inorganic compounds (metal, oxide and hydroxy salts) can be easily obtained in polyol media because of certain properties of such solvents: high boiling point, complexing, reducing, surfactant and amphiprotic characters [9–14]. We have demonstrated that two main reactions occur in these media, namely hydrolysis and reduction. The competition between these reactions may be easily controlled by the amount of water [15]. This new method allowed us to obtain monodispersed and equiaxed nanoparticles of the spinel $CoFe_2O_4$, close to 5 nm in size [16]. In contrast to similar nanoparticles prepared by other *chimie douce* routes [17–22] and the ball-milling method [23], the polyol-made nanoparticles exhibit high magnetization saturation at low temperature, close to that of the corresponding bulk material (80 versus 90 emu $g^{-1}$) and magnetic irreversibility up to room temperature. In order to determine the nature and the role of the various factors involved, and which lead to this promising behaviour, we have extended this method of synthesis to other spinel compounds, $MFe_2O_4$ (M = Ni, Zn, Mn,...).

We report here on the synthesis of $NiFe_2O_4$ nanoparticles and the study of their magnetic properties. Nickel ferrite is a typical soft ferromagnetic material, which crystallizes in a completely inverse spinel type with all nickel ions located in octahedral sites and iron ions occupying tetrahedral and octahedral sites. Several studies have been devoted to the synthesis and the magnetic properties of $NiFe_2O_4$ nanoparticles prepared by a great variety of chemical routes. A literature survey shows that the magnetic behaviour of these nanoparticles depends mainly on the synthesis route. The most common characteristic is their superparamagnetic behaviour and the reduction of the saturation magnetization in comparison with the corresponding bulk material (55 emu $g^{-1}$ [24]).

As will be shown below, the $NiFe_2O_4$ nanoparticles prepared in polyol medium behave similarly to $CoFe_2O_4$ ones. Their magnetization saturation is very high and close to that of bulk nickel ferrite. To better understand this singular feature and to underline the main advantages of this route, we have carried out several complementary analyses: x-ray diffraction (XRD), transmission electron microscopy (TEM), static and alternative (DC and AC) magnetic measurements, x-ray absorption (XAS), and zero-field and in-field Mössbauer spectrometry.

## 2. Experimental details

### *2.1. Preparation*

All chemicals were reagent grade and were used without further purification. Precursor salts, anhydrous $FeCl_3$ (Sigma) and $Ni(CH_3COO)_2{\cdot}4H_2O$ (Prolabo) in an atomic ratio of 4:3 were added to a given volume of 2-hydroxyethyl ether (diethylene glycol, DEG (Acros Organics)). The mixture was then heated to boiling (478 K). Two main parameters have to be controlled: the 'hydrolysis ratio', defined by the water to metal ratio, and the 'acetate ratio', defined by the acetate ion to metal ratio. $NiFe_2O_4$ nanoparticles were obtained when these two factors were fixed to 6.8 and 2.6, respectively, by adding sodium acetate trihydrate (Sigma). After cooling to room temperature, the particles were separated from the supernatant by centrifugation and washed with ethylene glycol to dissolve NaCl, then with acetone. The powders were dried in air at 325 K.

Two other polyols have been tested: ethylene glycol and propane-1,2-diol, but because they are stronger reducing agents than DEG, they led to the formation of a mixture of iron oxide and nickel metal particles.

### *2.2. Characterization*

X-ray diffraction (XRD) patterns were obtained with a Siemens D5000 diffractometer, using Fe K$\alpha$ radiation. They were recorded in the range 15°–115°($2\theta$) with a scan step of 0.025 ($2\theta$) for 10 s.

Particle morphology and chemical analysis of metal ions were determined by transmission electron microscopy (TEM) using a Jeol-100 CX II microscope equipped with an energy dispersive spectrometer (EDX), electron probe diameter 200 nm. To confirm the composition of the products, samples were dissolved in analytically pure hydrochloric acid. The ferrous and total iron contents were determined by potentiometric titration with cerium (IV) sulfate solution (Chem-Lab) and the nickel ion content by gravimetric titration using dimethylglyoxime [25].

Magnetic susceptibility and hysteresis loop measurements were made with a superconducting quantum interference device (SQUID) magnetometer. The DC magnetic susceptibility $\chi(T)$ was measured in zero-field cooling (ZFC) and field cooling (FC) modes in the 4.2–325 K range with an applied field, $H$, of 100 Oe. The variation of the magnetization with the field was obtained after cooling the sample to the measurement temperature in zero field and then increasing the field from 0 to 50 kOe. The same magnetometer was employed to obtain AC $\chi$ data (4.2–375 K) at various frequencies ($\nu = 2$, 20 and 200 Hz) with a field strength of 1 Oe. In all the cases, the powders were slightly compressed into the sampling tubes.

The $^{57}$Fe Mössbauer spectra were recorded in a transmission geometry using a $^{57}$Co/Rh $\gamma$-ray source mounted on an electromagnetic drive with a triangular velocity form. Spectra were obtained in zero magnetic field at 300 and 4.2 K and in a magnetic field of 6 T at 10 K. The Mössbauer spectra were analysed by a least-squares fitting method to Lorentzian functions. The isomer shifts ($\delta$) were referred to that of $\alpha$-Fe at 300 K. The sample (area, 3 cm$^2$) was prepared by dispersion of the compound (about 40 mg) in a specific resin.

Room-temperature XANES (x-ray absorption near edge spectroscopy) and low-temperature (10 K) EXAFS (extended x-ray absorption fine structure) data were collected for the Ni (8332.8 eV) K absorption edge of the nickel ferrite sample using a transmission mode detection scheme (optimized ion chambers) on the XAS13 beamline of the DCI storage ring at the French facility (LURE, Orsay). Data were also similarly collected on commercial powder sample $NiFe_2O_4$ (Alfa) as standard for Ni. The samples were ground and homogeneously dispersed in cellulose pellets enclosed in Kapton. XANES spectra were recorded using a Si(331) channel-cut monochromator with a 0.3 eV step size and normalized at the middle of the first EXAFS oscillation. EXAFS spectra were recorded using a Si(111) channel-cut monochromator with 2 eV steps. The data were analysed using the 'EXAFS pour le Mac' software package [26] with experimental amplitude and phase shift functions extracted from measurements on standard $NiFe_2O_4$.

## 3. Results

### *3.1. Phase analysis*

EDX and chemical analysis shows that the Ni/Fe ratio is very close to 0.5, and that there is no $Fe^{2+}$ cation. This is in good agreement with the stoichiometric formula, $NiFe_2O_4$. As was previously observed for different inorganic compounds prepared in polyol media (metal,

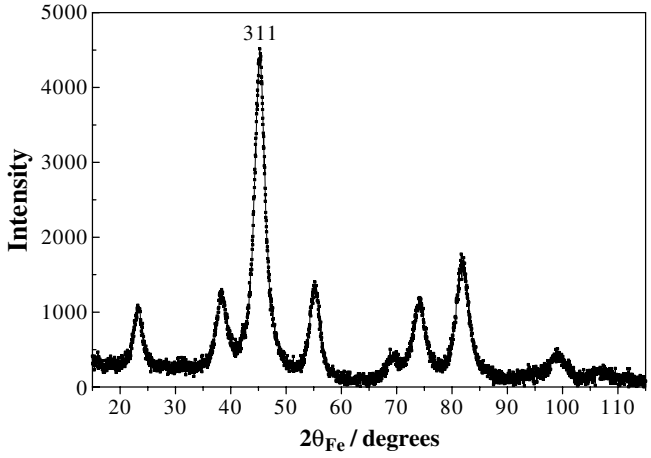


**Figure 1.** X-ray diffraction pattern of typical ultrafine $NiFe_2O_4$ particles prepared in DEG.

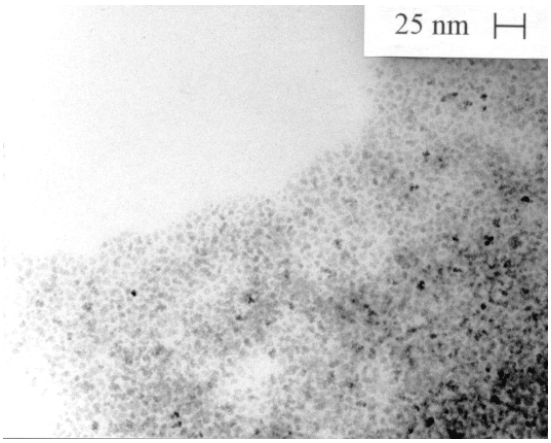


**Figure 2.** Transmission electron microscopy image of $NiFe_2O_4$.

hydroxy salts, oxide) [15], chemical analysis shows the presence of carbon (3%) due to organic species (acetate, polyol) adsorbed on the ferrite surface, as evidenced by infrared spectroscopy. These species appear to be strongly adsorbed on the oxide surface. The XRD pattern (see figure 1) reveals the formation of $NiFe_2O_4$ as a single phase. All the observed peaks belong to the spinel phase. The cell parameter inferred from UFIT refinements, $a = 8.356(2)$ Å, is slightly different from that of bulk material (8.338 Å) [27]. This may be attributed to the small size of the particles and their interface structure effects [28, 29]. This effect was already observed but not always explained for stoichiometric $NiFe_2O_4$ nanocrystals prepared by various *chimie douce* routes: polyvinyl alcohol sol–gel [30], hydrothermal [31] or co-precipitation [2] methods.

The average crystallite size estimated from the ferrite (311) peak and employing the Scherrer formula [32] is 4.4 nm.

TEM observations revealed almost spherical, nanoscale, non-agglomerated particles (figure 2). Their size lies in the nanometre range with a mean value of 2.8 nm, slightly

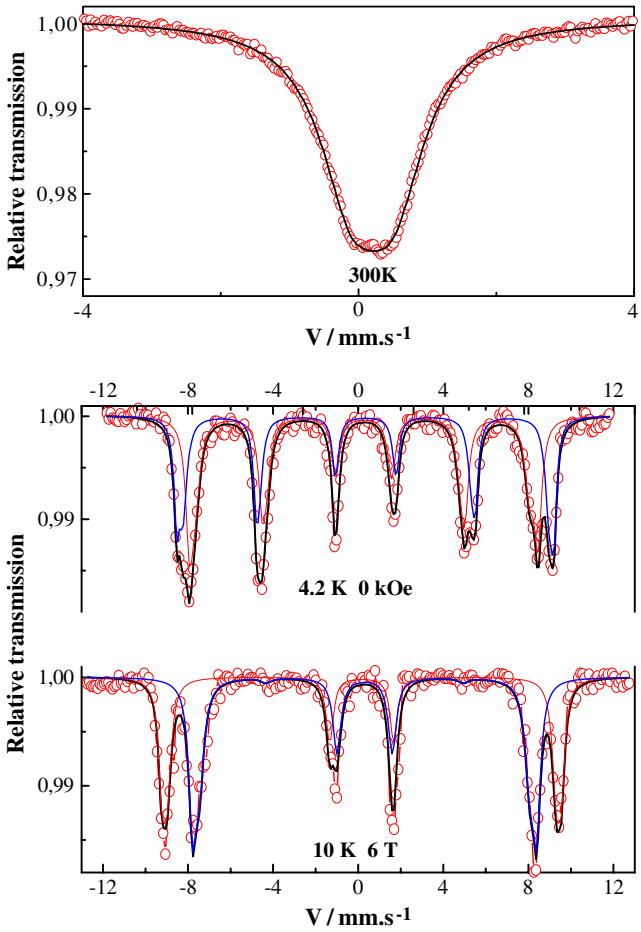


**Figure 3.** Room temperature and low-temperature zero-field and in-field (60 kOe) Mössbauer spectra of nickel ferrite nanoparticles. The temperature values are indicated on the figure.

lower than the XRD-determined average crystallite size. The difference is due to the mode of the size determination: by XRD it is assumed to be a volume distribution while by TEM it is assumed to be a radius one. This feature has been previously observed and reported [17]. Thus, it may be concluded that each nanoparticle consists of a single crystallite.

### *3.2. Mössbauer analysis*

As is shown in figure 3, the 4.2 K zero-field Mössbauer spectrum shows two weakly resolved sextets, attributed to tetrahedral and octahedral iron sites, while the 300 K Mössbauer spectrum consists of a broad quadrupolar feature typical of superparamagnetic relaxation effects. The lack of resolution prevents an accurate estimate of the importance of the latter. The 6 T-field Mössbauer spectrum shows two well resolved sextets with intermediate lines of near-zero intensity (see figure 3). This is consistent with a ferrimagnetic structure: the refinement allows us to attribute clearly the two sextets to tetrahedral and octahedral iron sites, according to the values of the isomer shift and to measure the $Fe_A^{3+}/Fe_B^{3+}$ population ratio. This ratio is found to be 0.75, which is too different from that observed for an exact inverse spinel structure

**Table 1.** Fitted Mössbauer parameters for two $Fe^{3+}$ components.

| Site | $B_{app}$ (T) | $\delta$ (mm s$^{-1}$) ±0.01 | $2\varepsilon$ (mm s$^{-1}$) ±0.01 | $B_{eff}$ (T) ±0.2 | $B_{hf}$ (T) ±0.2 | $\beta$ (deg) ±2 | Ratio (%) ±1 |
|---|---|---|---|---|---|---|---|
| $Fe^{3+}_A$ | 0 (4.2 K) | 0.40 | −0.03 | — | 49.7 | — | 0.54 |
| $Fe^{3+}_B$ | 0 (4.2 K) | 0.51 | 0.01 | — | 54.3 | — | 0.46 |
| $Fe^{3+}_A$ | 60 (10 K) | 0.40 | 0.00 | 57.1 | 51.1 | 0 | 0.43 |
| $Fe^{3+}_B$ | 60 (10 K) | 0.50 | 0.00 | 49.0 | 54.9 | 17 | 0.57 |

(1.00). Thus the cation distribution estimated from our spectrum corresponds to the formula $(Ni_{0.14}Fe_{0.86})[Ni_{0.86}Fe_{1.14}]O_4$, where the round and square brackets represent tetrahedral (A) and octahedral (B) spinel sites, respectively, establishing the presence of about 14% of nickel ions in tetrahedral sites. In addition, the in-field Mössbauer spectrum allows an estimate of both the effective fields $B_{eff}$ and the angles $\beta$ of the types of sites, where $B_{eff}$ corresponds to the vectorial sum of the hyperfine field $B_{hf}$ and the applied field $B_{app}$ and $\beta$ to the angle defined by the directions of the effective field for both tetrahedral and octahedral iron components and the $\gamma$-beam direction. The second step consists in calculating the hyperfine field $B_{hf}$ for both iron sites through the following relationship:

$$B^2_{hf} = B^2_{eff} + B^2_{app} - 2 * B_{eff} * B_{app} * \cos(\beta)$$

as $B_{app}$ is applied parallel to the $\gamma$-beam direction in our cryomagnetic device. The hyperfine field values for $Fe^{3+}$ in tetrahedral and octahedral sites are thus 51.1 and 55.1 T, respectively (table 1). It is important to note that these values are larger than those obtained from the zero-field Mössbauer spectrum, because of the presence of superparamagnetic relaxation effects which tend to lower the hyperfine field. Nevertheless, they are quite consistent with those reported earlier for bulk ferrite material ($H_A = 51.1$ T, $H_B = 55.3$ T) [33]. They differ from values observed for similar nanoparticles prepared by other methods: sonochemical method, $H_A = 50.0$ T and $H_B = 50.8$ T [3]; hydrothermal process, $H_A = 50.5$ T and $H_B = 51.3$ T [34], etc. Moreover, it has been observed that these values decrease when the particle size decreases. In the nanostructured particles prepared by high-energy ball-milling, the hyperfine field of $Fe^{3+}$ in tetrahedral and octahedral sites decreases from 48.8 to 47.6 T and from 51.5 to 50.3 T, respectively, when the particle size decreases from 60 to 10 nm [35].

### *3.3. EXAFS studies*

The local environment of nickel ions was investigated using x-ray absorption spectroscopy. The Ni K-edge XANES spectra of polyol-prepared $NiFe_2O_4$ powder and standard $NiFe_2O_4$ (Alfa) are shown in figure 4. In standard $NiFe_2O_4$, $Ni^{2+}$ cations are octahedrally coordinated by oxygen atoms in an inverse spinel-like structure. The intensity and shape of the main structure observed for prepared $NiFe_2O_4$ are in good agreement with the standard one, particularly in the pre-edge energy range (marked in figure 4), which confirms the 2+ oxidation state of nickel ions and that they are mainly octahedrally coordinated.

Figure 5 shows the Fourier-transformed (FT) Ni EXAFS data for the sample studied. The spectrum of standard $NiFe_2O_4$ is included in figure 5 for comparison. For bulk $NiFe_2O_4$, the FT curve consists of three peaks at 1.67, 2.58 and 3.10 Å in the 0–4 Å $R$-range (phase shift uncorrected). The first peak corresponds to Ni–O bonds, the second to the Ni–$M_B$ and the third to Ni–$M_A$ and Ni–O, where $M_B$ is the metal ion located in B spinel sites and $M_A$ in A ones. By analogy, it is possible to identify the different coordination shells of nickel atoms in the

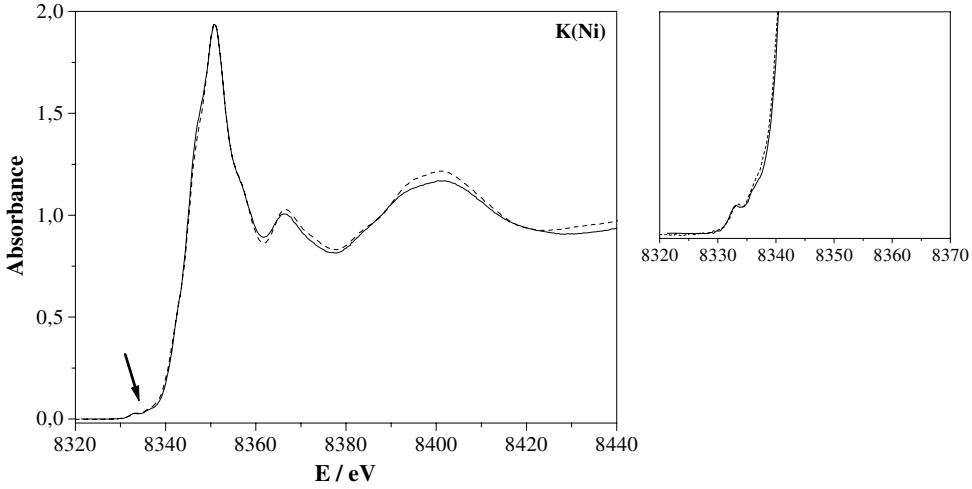


**Figure 4.** XANES spectra of $NiFe_2O_4$ nanoparticles (dashed curve) and standard $NiFe_2O_4$ (full curve). Zoom of the pre-edge region is reported in the right window.

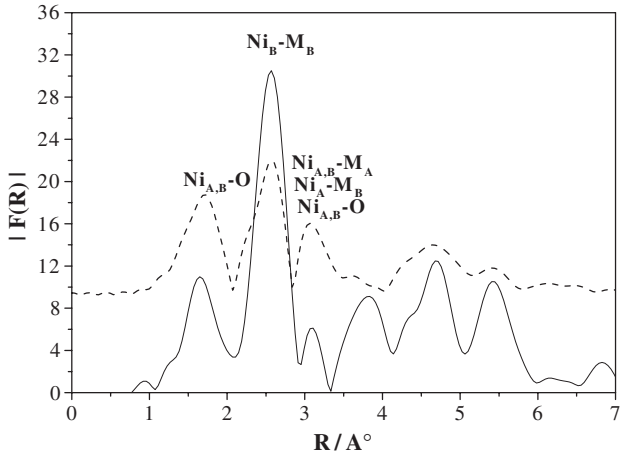


**Figure 5.** Modulus of the $k^3$-weighted Fourier transform of Ni EXAFS data for samples prepared in polyol (dashed curve) and standard $NiFe_2O_4$ (full curve).

nanoparticles. Three well resolved peaks are present. The positions of the FT Ni EXAFS peaks in our material are close to those observed with standard $NiFe_2O_4$ (inverse spinel); however, their amplitudes are different:

(i) the total FT have a reduced amplitude suggesting the formation of small particles and
(ii) the third peak whose centroid appears at 3.10 Å, which is mainly related to the tetrahedral/tetrahedral and tetrahedral/octahedral metal correlations, have an enhanced amplitude suggesting that the absorbing species reside partly in the tetrahedral spinel sites.

The structural parameters obtained by modelling the first coordination sphere at the Ni K-edge according to two different assumptions: (i) nickel ions in octahedral sites and (ii) nickel

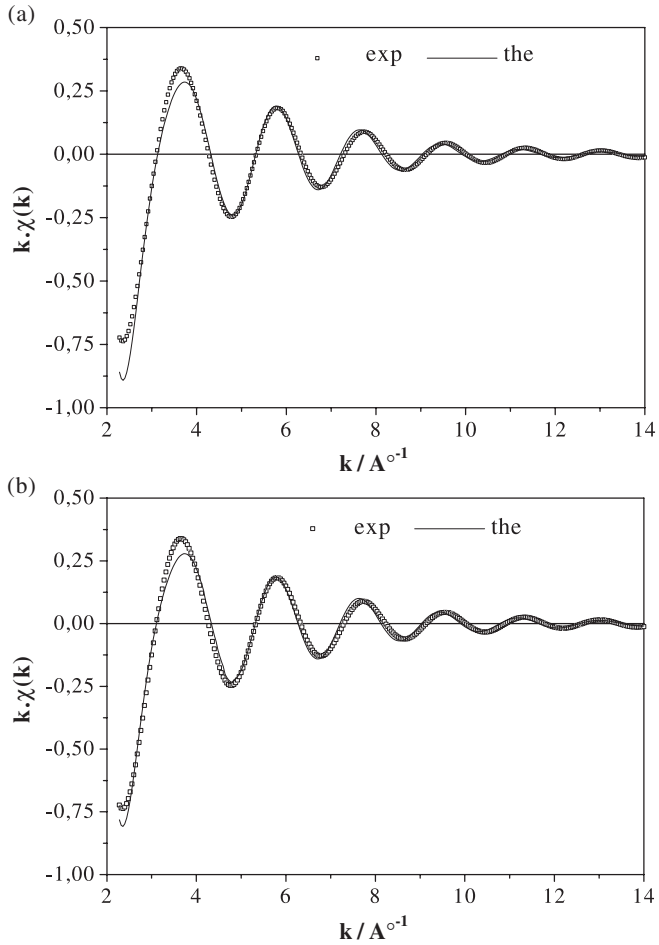


**Figure 6.** Inverse Fourier transform of the first peak at the Ni K-edge for $NiFe_2O_4$: (a) fitting with an octahedral first coordination sphere and (b) fitting with both octahedral and tetrahedral first coordination spheres.

ions in octahedral and tetrahedral sites, are listed in table 2. The corresponding curves are presented in figure 6. The curve fit based on second hypothesis, with both $Ni_A$–O and $Ni_B$–O pair contributions in the first coordination sphere of Ni, was the better (the residual fit factor decreases). Furthermore, the $Ni_B$–O (2.05 Å) obtained is in good agreement with that observed for bulk $NiFe_2O_4$ [27], and the $Ni_A$–O distance (1.93 Å) agrees fairly well with that inferred from the bond valence parameters for solids developed by Brese *et al* [36]. Obviously, the intermediate $N$ value, which measures the number of oxygen atoms at 2.05 Å, obtained for the $Ni_B$–O pair (5.6) compared to the bulk-like $NiFe_2O_4$ one (6) allows us to estimate the proportion of nickel atoms in each spinel site, which is about 10% in A, and 90% in B, respectively, in fair agreement with the Mössbauer results.

### *3.4. Magnetic measurements*

Figure 7 shows the DC magnetic susceptibility $\chi$ measured upon warming after zero-field cooling or field cooling (ZFC and FC, respectively) at an applied DC field of 100 Oe. The

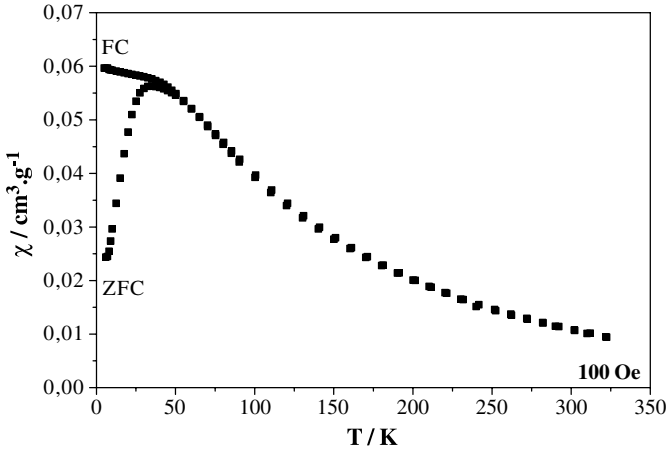


**Figure 7.** DC susceptibility measured in FC and ZFC modes for $NiFe_2O_4$ from 4.5 to 325 K.

**Table 2.** EXAFS results at the Ni K-edge of $NiFe_2O_4$ nanocrystals. $N$, the number of back-scatterers at a distance $R$ from the central atom and $\sigma$ the Gaussian Debye–Waller factor associated with $R$. The energy threshold, $E_0$, taken at the first inflexion of the Ni absorption edge is corrected in the fitting procedure by the $\Delta E_0$ parameter.

| $Ni_B$–O | | | | $Ni_A$–O | | | | |
|---|---|---|---|---|---|---|---|---|
| $N_1$ | $R$ (Å) | $\Delta E_0$ (eV) | $\sigma^2$ (Å$^2$) | $N_2$ | $R$ (Å) | $\Delta E_0$ (eV) | $\sigma^2$ (Å$^2$) | $\rho$ |
| 6.0 | 2.05 | 1.88 | $4.3 \times 10^{-3}$ | — | — | — | — | 0.040 |
| 5.6 | 2.05 | 1.83 | $2.8 \times 10^{-3}$ | 0.4 | 1.93 | 1.83 | $3.7 \times 10^{-3}$ | 0.021 |

FC and ZFC curves are clearly distinguishable. Zero-field cooling leads to a susceptibility maximum at $T_f$, around 50 K (at which the spins freeze and order), while field cooling leads to slowly decreasing values below this temperature.

A plot of AC susceptibility showing the in-phase component ($\chi'$) and the out-of-phase ($\chi''$) as a function of the temperature from 4.2 to 375 K is given in figure 8, for frequencies from 2 Hz to 200 kHz. The susceptibilities presented in terms of mass susceptibility (emu $g^{-1}$, cgs) were measured under an AC magnetic field strength of 1 Oe. Broad maxima appear at temperatures from 50 to 80 K in both in-phase $\chi'$ and out-of-phase $\chi''$ susceptibility. This temperature is frequency-dependent and increases with increasing frequency for both components. For instance, in the case of $\chi'$, it increases from 69 K at 2 Hz to 79 K at 200 Hz. At $T > 80$ K, the $\chi'$ curves superpose perfectly, and $\chi''$ are zero, signifying thermodynamic equilibrium in this higher temperature range [37]. A non-zero $\chi''$ at low temperature ($30 < T < 80$) points to the existence of ferrimagnetic behaviour and remanence.

Figure 9 displays the first magnetization as a function of the applied field measured at temperatures from 4.2 to 300 K. For each temperature, saturation is reached at less than 50 kOe. The saturation magnetization decreases from 51.3 to 38.0 emu $g^{-1}$ when the temperature goes from 4.2 to 300 K.

Below the freezing or ordering temperature, magnetic irreversibility is observed, as shown by the occurrence of hysteresis phenomena (see figure 10). The full loop obtained at 5 K reveals that the material exhibits remanence and coercivity. The low inferred values of squareness and coercivity (0.12 and 95 Oe, respectively) are in agreement with the well established soft magnetic character of $NiFe_2O_4$.

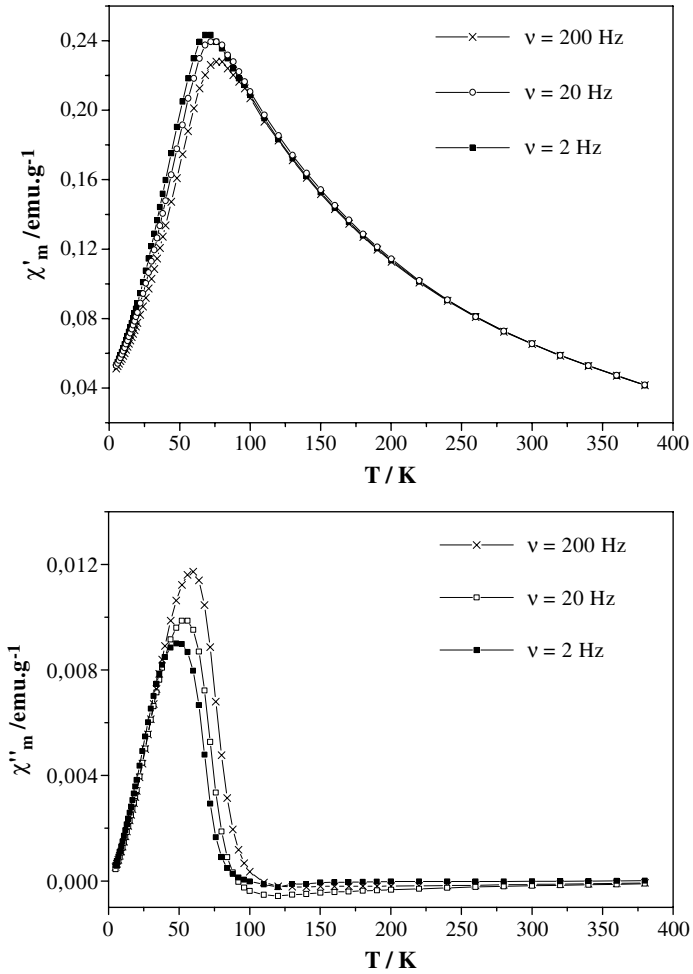


**Figure 8.** Real ($\chi'_{\mathrm{m}}$) and imaginary ($\chi''_{\mathrm{m}}$) parts of AC susceptibility for $NiFe_2O_4$ measured at different frequencies in zero field.

The particle size has also been inferred from magnetic data using the Langevin function, i.e. $M(D) = \mathrm{Ms}\{\coth(\mu H/kT)–(kT/\mu H)\}$ with $\mu = \mu(D)Ms\pi D^3/6$, where Ms and $Ms$ are the total saturation of the overall particle and of the bulk material, respectively. For a given field $H$ and temperature $T$, $M(D)$ is the magnetization of particle characterized by the diameter $D$ [38]. Good agreement is obtained between the simulated and observed magnetic curves, $M = f(H/T)$ (figure 9). The mean particle size $D$ inferred from these simulations (3 nm) is in good agreement with the that obtained from TEM and XRD data.

## 4. Discussion

Altogether, these results may indicate the occurrence of a spin-glass thermodynamic transition [39] or/and superparamagnetism [40].

Spin-glass has previously been evidenced in nanostructured $NiFe_2O_4$ powders prepared by ball-milling. These particles exhibit remarkable high-field irreversibility, the hysteresis loop

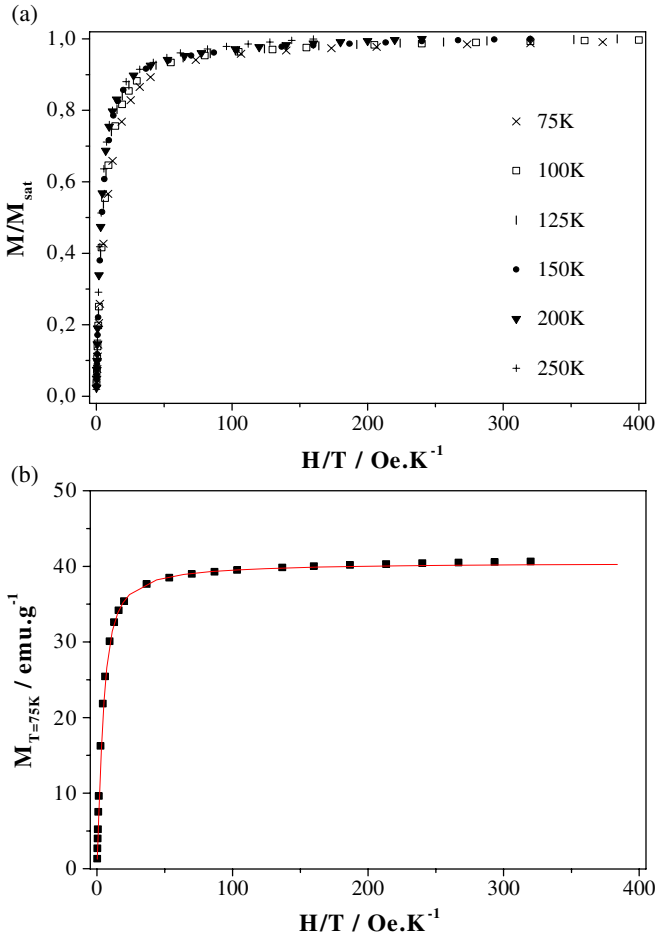


**Figure 9.** (a) $M/M_{\text{sat}}$ versus $H/T$, as measured at temperatures higher than 50 K described by the Langevin function. (b) Illustration of the Langevin fit for $T = 125$ K.

remaining open up to 160 kOe [41]. Similar results were obtained by Chinnasamy *et al* [35] for nickel ferrites also prepared by ball-milling and by Berkowitz *et al* for fine coated nickel ferrite particles prepared by ball-milling [42]. This high irreversibility has also been observed for $\gamma$ $Fe_2O_3$ prepared by co-precipitation in alkaline medium followed by gentle heat treatment at 523 K in air. Complete saturation is not reached for the smallest particles (3.5 nm) even for an applied field of 55 kOe [43]. This high-field irreversibility, which increases when the particle size decreases, occurs along with low magnetization compared to the corresponding bulk material. To account for these anomalous properties Kodama *et al* developed a model of magnetization within the particles consisting of ferrimagnetically aligned core spins and a spin-glass-like surface layer [44].

The nanoparticles prepared in polyol present a significant different magnetic behaviour. Although irreversibility is observed, the field at which it vanishes is rather low. This suggests superparamagnetism-like behaviour rather than a spin-glass-like one. To distinguish between these two phenomena, the frequency shift per decade of the maximum of in-phase AC susceptibility versus $T$ was used. The value observed for $\Delta T_{\text{f}}/(T_{\text{f}}\Delta(2\pi\nu))$ is of the order of

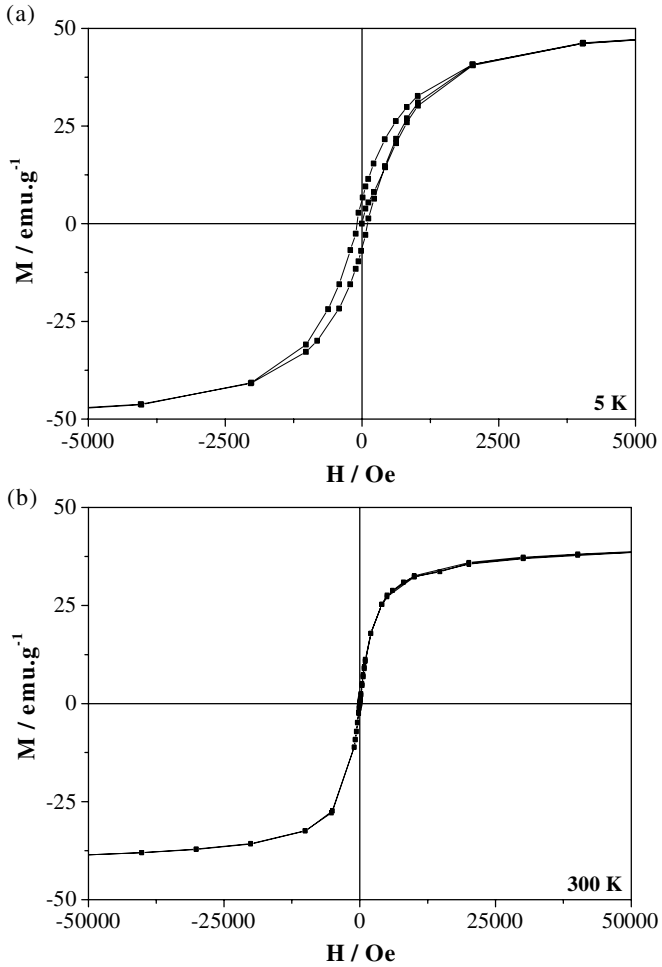


**Figure 10.** Isothermal hysteresis loop of $NiFe_2O_4$ powder at (a) 5 K and (b) 300 K.

$10^{-1}$ which is quite similar to those found for superparamagnetic systems [45]. Furthermore, the magnetization curves for $T > 50$ K can be well described using the Langevin function, confirming the presence of superparamagnetic relaxation effects.

The absence of an important spin-glass like surface layer is also evidenced by the observed high magnetization value. This magnetization at 5 K is close to that of the corresponding bulk material (51.3 emu $g^{-1}$ compared to 55 emu $g^{-1}$) and remains high (38.0 emu $g^{-1}$) at RT. Except for the study on nanostructured powders by Chinnasamy *et al* [35], to the best of our knowledge the superparamagnetic nanoparticles prepared in polyol medium present a very high magnetization never previously observed for particles of similar size obtained by other routes, which conversely lead to very low magnetization values compared to the bulk one (see table 3). This has been attributed to the occurrence of magnetic disorder within particles not made by the polyol method. Two disorder types have been postulated. The first involves a ferrimagnetically aligned spin core surrounded by a magnetic disorder surface called the dead layer [44]. The second disorder type occurs in the whole volume of the particle [43]. It should be noted that ball-milling, even if it leads to low magnetization, differs from the *chimie douce*

**Table 3.** Comparison of the blocking temperature $T_B$, saturation magnetization and reduced remanence of $NiFe_2O_4$ nanoparticles obtained by different methods.

| Reference | Synthesis method of $NiFe_2O_4$ nanocrystals | Size (nm) | $T_B$ (K) | $M_{sat}$ (emu $g^{-1}$) |
|---|---|---|---|---|
| This work | Forced hydrolysis in polyol at 473 K | 2.8 | 50 (0.2 kOe) | 51 (5 K)<br>38 (300 K) |
| [2] | Co-precipitation | | Not given | ≈3 (300 K) |
| [50] | Aqueous oxidative precipitation | 6<br>20 | Not given | 3 (300 K)<br>23 (300 K) |
| [51] | Sonochemical decomposition of solution of volatile carbonyl precursors at 273 K | 7 | Not given | 5 (300 K) |
| [52] | Shock wave treatment of nanosized mixed powders of ferric oxide and nickel oxide prepared by co-precipitation | <10 | Not given | 13.7 (293 K) |
| [35] | Ball-milled (30 h) bulk ferrite prepared by conventional ceramic route | 10 | 30 (90 kOe) | 38 (5 K) |
| [48] | Co-precipitation followed by heat treatment at low temperature | 25 | >300 | 32.6 (77 K) |
| [53] | RF plasma deposition | <55 | >300 | 19 (5 K) |
| [54] | Co-precipitation/mechanical alloying | 10 | Not given | 6.9 (300 K) |

routes described in the literature. Such a process gives rise to high irreversibility and interface anisotropy, since the resulting ferrite particles are structurally and magnetically disordered due to changes in the degree of inversion, the creation of oxygen vacancies and amorphization of the structure [46, 47].

Mössbauer and XAS studies provide interesting results which partly explain the enhancement of the magnetization observed here. As discussed in the results section, a Mössbauer study in an external field of 6 T reveals a departure from the thermodynamically stable spinel phase structure (inverted structure) encountered for $NiFe_2O_4$: about 14% of the $Ni^{2+}$ are forced into the tetrahedral (A) sites and an equal amount of $Fe^{3+}$ moves from tetrahedral to octahedral (B) sites. This results in an increase in the magnetization, if we assume collinear ferrimagnetic interaction between magnetic cations in octahedral and tetrahedral sites; this hypothesis is confirmed by in-field Mössbauer results as discussed hereafter.

The departure from the inverted structure was confirmed by the XAS study. The amplitudes of the FT Ni EXAFS peaks are different from those observed in standard $NiFe_2O_4$, i.e. in particular, the third peak related to tetrahedral/tetrahedral and tetrahedral/octahedral metal correlations has an enhanced amplitude, suggesting that nickel cations are partly located in the tetrahedral sites. To the best of our knowledge, the influence of the cation distribution on the magnetic properties of $NiFe_2O_4$ nanoparticles was previously discussed only in the case of ball-milled nanostructured powders [35].

The collinearity of the magnetic structure can be followed by in-field Mössbauer spectra through the intensities of the second and fifth lines. With our cryomagnetic device ($\gamma$ radiation parallel to external field), zero and non-zero intensity lines are consistent with collinear and non-canted iron magnetic moments. The present results differ from those obtained on ball-milled nanostructured powders, i.e. an increase in the line intensities when the grain size decreases, which is ascribed to the increase of the canting of the $Fe^{3+}$ spins with respect to the applied field. Similar results have been obtained for ultrafine $NiFe_2O_4$ prepared by a chemical route [48]. In these cases, the canting angle increases from about 14° to 34° when the particle

size decreases from 60 to 10 nm. The authors concluded that this phenomena may be due to surface effects, where the spins on the surface layer are canted. This observation accounts for the model of ferrimagnetic core spins surrounded by a spin-glass-like surface layer [44]. In addition, it explains very well the decrease in the magnetization for the nanoparticles reported in the literature. It should be noted that the canting angle of 14° for 60 nm particles made by ball-milling may be considered as negligible (inoperative) since the saturation magnetization observed (60 emu $g^{-1}$) is very close to that of bulk $NiFe_2O_4$ (55 emu $g^{-1}$). Furthermore, careful examination of the in-field spectrum of the corresponding sample reveals that the second and fifth lines have almost zero intensities.

Despite their small size, about 3 nm, the nanoparticles prepared in polyol behave similarly to the 60 nm nanoparticles described above. Their saturation magnetization is very high (51.3 emu $g^{-1}$). Furthermore, the in-field Mössbauer measurements show that the canting angle is close to zero for $Fe^{3+}$ in tetrahedral sites and very low (17°) for $Fe^{3+}$ in octahedral sites. This leads to an in-field Mössbauer spectrum with a vanishing intensity of the second and fifth lines (figure 3).

The results discussed above on $NiFe_2O_4$ along with those previously published on $CoFe_2O_4$ indicate a rather surprising behaviour of spinel nanoparticles prepared in polyol compared to those obtained by other *chimie douce* routes. Indeed, while these latter methods led to low magnetization saturation and canting effects, working in polyol avoids these disadvantages, the nanoparticles obtained in this way show promising properties: high magnetization saturation, absence of canting and hyperfine field close to that of the bulk material. Such interesting behaviour appears to be clearly related to two main factors: good crystallinity of the nanoparticles and the departure from the classical cation distribution in the spinel structure. The last factor is due to reducing the size of the particle down to the nanometre range. The good crystallinity, which means the absence of significant structural defects, is favoured by the thermal conditions employed in this new synthesis method. The nanoparticles are here prepared at relatively high temperature (478 K) and under thermal conditions close to those used in the hydrothermal method. Recently Caruntu *et al* [49] confirmed such good crystallinity by TEM observation in the case of $MnFe_2O_4$-capped nanoparticles obtained via a route involving hydrolysis in polyol followed by complexation with oleic acid.

## 5. Conclusion

Among various methods of fabricating ferrite nanoparticles (of nickel and cobalt), the forced hydrolysis of metal salts in polyol appears as an attractive *chimie douce* route which provides monodisperse particles showing surprisingly good crystallinity and enhanced magnetic characteristics. Similar results are also observed for zinc and manganese ferrites (details of these results will be published elsewhere). The nanoparticles obtained exhibit a high saturation magnetization value at low temperature close to that of the bulk material, despite their nanometric size. This value is consistent with almost perfectly magnetically ordered single-domain particles without a significant dead magnetic layer and a cation distribution slightly different from the thermodynamically stable inverse spinel structure. This behaviour, which is promising if such materials are to be used in technological applications, has never been observed for similar particles obtained by other routes. It should, however, be noted that the nanoparticles remain superparamagnetic down to 50 and 300 K for nickel and cobalt, respectively. Work is in progress to increase the blocking temperature, which would make these nanomaterials serious candidates for high-density recording applications, for instance. In this context two parameters are of particular interest: (i) partial substitution of the Fe(III)

cation by lanthanide with high magnetocrystalline anisotropy and (ii) increase in the particle size by controlling nucleation and growth in the polyol.

## Acknowledgment

The authors thank Dr Patrick Gredin and Dr Patricia Beaunier, from the University of Paris 6 (France), for XRD facilities and TEM analysis.

## References

[1] Goya G F and Rechenberg H R 1999 *J. Magn. Magn. Mater.* **196/197** 191
[2] Sato T, Iijima T, Seki M and Inagaki N 1987 *J. Magn. Magn. Mater.* **65** 252
[3] Shafi K V P M, Koltypin Y, Gedanken A, Prozorov R, Balogh J, Lendvai J and Felner I 1997 *Phys. Chem.* B **101** 6409
[4] Vollath D, Szabo D V, Taylor R D and Willis J O 1997 *J. Mater. Res.* **12** 2175
[5] Wang J, Chong P F, Ng S C and Gan L M 1997 *Mater. Lett.* **30** 217
[6] Sanchez C and Livage J 1990 *New J. Chem.* **14** 513
[7] Chen D H and He X R 2001 *Mater. Res. Bull.* **36** 1369
[8] Cabanas A and Poliakoff M 2001 *J. Mater. Chem.* **11** 1408
[9] Fiévet F, Lagier J P and Figlarz M 1989 *Mater. Res. Soc. Bull.* **14** 29
[10] Silvert P Y and Tekaia-Elhsissen K 1995 *Solid State Ion.* **82** 53
[11] Toneguzzo P, Viau G, Acher O, Fiévet-Vincent F and Fiévet F 1998 *Adv. Mater.* **10** 1032
[12] Collins I R and Taylor S E 1992 *J. Mater. Chem.* **2** 1277
[13] Jezequel D, Guenot J, Jouini N and Fiévet F 1995 *J. Mater. Res.* **10** 77
[14] Poul L, Jouini N and Fiévet F 2000 *Chem. Mater.* **12** 3123
[15] Poul L, Ammar S, Jouini N, Fiévet F and Villain F 2003 *J. Sol–Gel Sci. Technol.* **26** 261
[16] Ammar S, Helfen A, Jouini N, Fiévet F, Villain F, Rosenman I, Danot M and Molinié P 2001 *J. Mater. Chem.* **1** 186
[17] Moumen N and Pileni M-P 1996 *Chem. Mater.* **8** 1128
[18] Blaskov V, Petkov V, Rusanov V, Martinez L I M, Martinez B, Munoz J S and Mikhov M 1996 *J. Magn. Magn. Mater.* **162** 331
[19] Cheng F X, Peng Z Y, Liao C S, Xu Z G, Gao S and Yan C H 1996 *Solid State Commun.* **107** 471
[20] Lee J G, Park J Y and Kim C S 1998 *J. Mater. Sci.* **33** 3965
[21] Grigorova M, Blythe H J, Blaskov V, Rusanov V, Petkov V, Masheva V, Nihtianova D, Martinez L I M, Munoz J S and Mikhov L 1998 *J. Magn. Magn. Mater.* **193** 163
[22] Seip C T, Carpenter E E and O'Connor C J 1998 *IEEE Trans. Magn.* **34** 1111
[23] Todaka Y, Nakamura M, Hattori S, Tsuchiya K and Umemoto M 2002 *Nippon Kinzoku Gakkaishi* **66** 34
[24] Valenzuela R 1994 *Magnetic Ceramics* (Cambridge: Cambridge University Press)
[25] Charlot G 1961 *Les Méthodes de la Chimie Analytique, Analyse Quantitative Minéale* (Paris: Masson and Cie)
[26] Michalovich A 1991 *Logiciels Pour la Chimie* (Paris: La société Française de Chimie)
[27] Subramanyam K N 1971 *J. Phys. C: Solid State Phys.* **4** 2266
[28] Sarrazin P, Bernard F, Calvarin G, Niepce J C and Thierry B 1998 *J. Physique Coll.* IV **8** 85
[29] Bellin T, Guigue-Millot N, Caillot T, Aymes D and Niepce J C 2002 *J. Solid State Chem.* **163** 459
[30] Wang L and Li F S 2001 *J. Magn. Magn. Mater.* **223** 233
[31] Yi X, Yitai Q, Jing L, Zuyao C and Li Y 1995 *Mater. Sci. Eng.* B **24** L1
[32] Warren E 1969 *X-ray Diffraction* (Reading, MA: Addison-Wesley)
[33] Leung L K, Evans B J and Morrish A H 1973 *Phys. Rev.* B **8** 29
[34] Pannaparayil T, Marande R, Komarneni S and Sankar S G 1988 *J. Appl. Phys.* **64** 5641
[35] Chinnasamy C N, Narayanasamy A, Ponpandian N, Chattopadhyay K, Shinoda K, Jeyadevan B, Tohji K, Nakatsuka K, Furubayashi T and Nakatani I 2001 *Phys. Rev.* B **63** 184108
[36] Brese N E and O'Keeffe M 1991 *Acta Crystallogr.* B **47** 192
[37] Huser D 1983 *Phys. Rev.* B **27** 3100
[38] Charles S W and Popplewell J 1982 *Ferromagnetic Materials* (Amsterdam: North-Holland)
[39] Dormann J L and Noguès M 1991 *Phase Transit.* **33** 159
[40] El-Hilo M, O'Grady K and Chantrell R W 1992 *J. Magn. Magn. Mater.* **114** 307
[41] Kodama R H, Berkowitz A E, McNiff E J, Foner J and Foner S 1997 *J. Appl. Phys.* **81** 5552

[42] Berkowitz A E, Lahut J A and van Buren C E 1980 *IEEE Trans. Magn.* **16** 184
[43] Morales M P, Veintemillas-Verdaguer S, Montero M I, Serna C J, Roig A, Casas L, Martinez B and Sandiumenge F 1999 *Chem. Mater.* **11** 3058
[44] Kodama R H 1999 *J. Magn. Magn. Mater.* **200** 359
[45] Bruner M 1995 *PhD Thesis* University of Zürich
[46] Battle J, Clark T and Evans B J 1997 *J. Phys. Coll.* IV **7** 257
[47] Hamdeh H H, Ho J C, Oliver S A, Willey R J, Oliveri G and Busca G 1997 *J. Appl. Phys.* **81** 1851
[48] Morrish A H and Haneda K 1981 *J. Appl. Phys.* **52** 2496
[49] Caruntu D, Remond Y, Chou N H, Jun M J, Caruntu G, He J, Goloverda G, O'Connor C and Kolesnichenko V 2002 *Inorg. Chem.* **41** 6137
[50] Rajendran M, Bhattacharya A K, Das D, Chintalapudi S N and Majumdar C K 2001 *Int. J. Mod. Phys.* B **15** 305
[51] Kurikka V P M S, Koltypin Y and Gedanken A 1997 *J. Phys. Chem.* B **101** 6409
[52] Liu J, He H, Jin X, Hao Z and Hu Z 2001 *Mater. Res. Bull.* **36** 2357
[53] De Marco M, Wang X W, Snyder R L, Simmins J, Bayya S, White M and Naughton M J 1993 *J. Appl. Phys.* **73** 6287
[54] Shi Y, Ding J, Liu X and Wang J 1999 *J. Magn. Magn. Mater.* **205** 249